JOURNAL OF MATERIALS SCIENCE 18 (1983) 1455–1465

The cohesive and adhesive strength of ice

E. H. ANDREWS, N. A. LOCKINGTON
Department of Materials, Queen Mary College, London E1 4NS, UK

The plane-strain fracture-energy test developed by Andrews and Stevenson has been applied to the study of ice adhering to substrates of stainless steel, titanium and anodised aluminium. In most cases the fracture is cohesive through the ice, and therefore yields a cohesive fracture energy (critical energy release rate). The value of this fracture energy, however, is dependent upon the nature of the substrate, stainless steel giving significantly lower values than titanium. The fracture energy is also affected by the rate of formation of the ice and by the rate of testing. Many of these effects can be traced to the influence of the substrate on the air-bubble content of the ice layer. At testing temperatures approaching the melting point of ice, a transition in fracture mode is observed from cohesive to adhesive, and the fracture energy diminishes. The addition of small amounts of sodium fluoride to the water from which the ice is formed, lowers the transition temperature to -5° C, and emphasizes the transition to the adhesive failure mode.

1. Introduction

While the strength of ice itself is of interest to glaciologists, the adhesion of ice to metals is of greater concern to those involved with the operation of civil, nautical and aeronautical structures in low-temperature environments. The present work was undertaken in the latter context and has as its ultimate object the improvement of ice release from surfaces. However, our recent studies on the mechanics of adhesion [1–3], demonstrate clearly that the cohesive strength of an adhering substance has a direct bearing upon its adhesive properties. It is highly desirable, therefore, to study adhesive and cohesive strengths simultaneously as well as any transitions that may occur between these two modes as the conditions of test are varied.

The plane-strain fracture test devised by Andrews and Stevenson [4] lends itself to such a study and has the further advantage of being simple to perform. In this test the substance to be studied is cast on the chosen substrate in such a way as to include a circular non-adhering disc of plastic at the interface. This disc thus creates a totally enclosed defect which can be propagated as a crack by the application of pressure through an access port in the substrate. The fracture conditions are ideally plane-strain, simply because the crack is totally enclosed, and any interfacial fracture is also unaffected by stresses set up by differential contraction of the adhesive and substrate materials. The critical energy release rate, or fracture energy, can be readily derived from the critical pressure for fracture and the dimensions of the specimen [4].

The cohesive strength of ice has been investigated by many workers, and is found to depend strongly on the technique employed and the testing conditions [5–9]. Even when care has been taken to minimize errors, a wide scatter commonly occurs in the data and one of the advantages of the test employed here is its good reproducibility. Because ice exhibits creep under load, it is important that fracture tests be carried out at different rates [8], and this is achieved in the present work by varying the rate of pressurization. The fracture mechanics approach adopted in this work has not been widely used in the study of ice, but Goodman and Tabor [10] and Goodman [11] measured fracture energy using the three-point bending of sharply notched beams, as well as by a diamond indentation test, while Liu and Miller [12] carried out tests at different rates on "compact tension" specimens.

The adhesive properties of ice have been reviewed by Jellinek [13], who used the idea that

0022–2461/83 $03.00 + .12

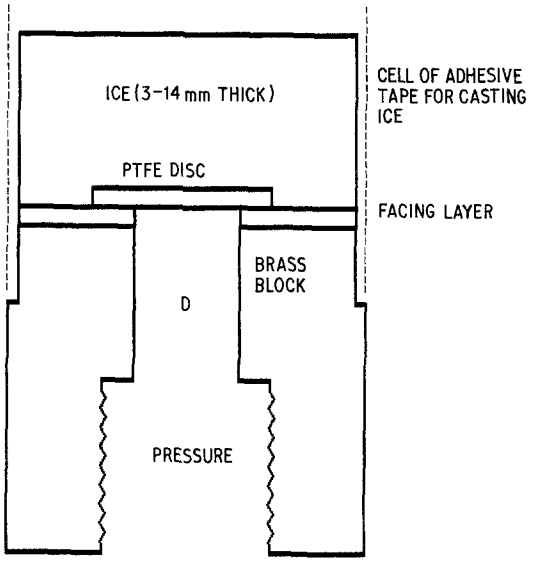

Figure 1 Test specimen.

a liquid-like transition layer exists at the ice/solid interface to explain the characteristics of ice adhesion. This concept is particularly useful in accounting for the differences between tensile and shear modes of adhesive testing and the transition from cohesive to adhesive failure with rising temperature.

2. Experimental method

The test method and apparatus have been described fully elsewhere [4]. The specimen is of the form shown in Fig. 1 and pressure is applied through the access port D to produce fracture. The pressure is monitored continuously on a high speed UV recorder from which both the peak pressure and the time-to-fracture can therefore be read. The fracture energy, or critical energy release rate, is then given by one of the following formulae.

For cohesive fracture through the ice;

$$2\mathcal{T} = P_c^2 c/E f_1 (h/c). \quad (1)$$

For adhesive fracture along the interface;

$$\theta = P_c^2 c/E f_2 (h/c). \quad (2)$$

The parameters $2\mathcal{T}$ and θ are completely equivalent, being the energy required to create unit area of new crack plane during propagation of failure. Different symbols are used, however, to differentiate between cohesive and adhesive failure events as a matter of convenience. Both $2\mathcal{T}$ and θ are formally equivalent to the critical energy release rate of linear fracture mechanics. The other quantities appearing in Equations 1 and 2 are: P_c, the critical pressure for failure; c, the radius of the artificial flaw; E, Young's modulus of ice; h the height of the ice above the flaw; and

$$f_1 = \frac{1}{1-\nu^2}\left\{\frac{3}{32}\left[\left(\frac{c}{h}\right)^3 + \left(\frac{c}{h}\right)\frac{4}{1-\nu}\right] + \frac{1}{\pi}\right\}^{-1} \quad (3)$$

$$f_2 = \frac{1}{1-\nu^2}\left\{\frac{3}{32}\left[\left(\frac{c}{h}\right)^3 + \left(\frac{c}{h}\right)\frac{4}{1-\nu}\right] + \frac{2}{\pi}\right\}^{-1} \quad (4)$$

where ν is Poisson's ratio of ice. The derivation of these equations will be found in Andrews and Stevenson [4].

Values for E and ν determined by various investigators have varied widely [14]. Most recent measurements of E indicate its value to lie in the range 8.34 to 8.76 GN m^{-2} [7, 9] and we shall assume a value of 8.50 GN m^{-2} for temperatures above -20° C. The Young's modulus of ice increases linearly by some 18% as the temperature falls from -10 to -180° C, and this would indicate a difference in E of some 2% between -5 and -20° C. We shall ignore this small difference. Values quoted for Poisson's ratio vary from 0.31 to 0.40 and we shall use the value 0.35. It will be noted that the analysis gives fracture energies rather than critical stress intensity factors, K_{IC}. For those more familiar with the latter quantity, we give the following conversion data.

$$K_{IC} = [2E\mathcal{T}/(1-\nu^2)]^{1/2} \text{ (plane strain)}$$
$$= 3.1\,(2\mathcal{T})^{1/2} \text{ GN m}^{-3/2}$$

for ice when $2\mathcal{T}$ is given in J m^{-2}.

The fracture specimens were prepared by freezing distilled water (which had been boiled to reduce the amount of dissolved air), on to the end faces of metal cylinders (the substrates of Fig. 1). This was achieved by forming temporary moulds of adhesive tape around the cylinders into which the water was poured to whatever height was desired. Additionally, some tests were carried out using unboiled water, tap water and dilute salt solutions.

The metal substrates were either commercially pure Ti or brass blocks surfaced with a thin sheet of 18/8 stainless steel. A smaller number of tests were carried out on anodised aluminium substrates. Before casting the ice, the metal surfaces were prepared on 220 grit silicon carbide paper, cleaned with carbon tetrachloride and rinsed in

acetone. The access port in the substrate blocks was then covered with a PTFE disc, 250 μm thick, which forms the enclosed crack once the ice has been cast. Although the "crack" is blunt-edged, it acts like a true crack because a sharp 90° angle is formed where its end meets its major surfaces.

The ice-making temperature was a variable in these experiments, and the substrates were held at the selected temperature in a refrigerator for at least 1 h before ice was cast. Specimens were kept at the ice-making temperature for several hours before being raised or lowered to the testing temperature, which was also variable. The testing temperature was also held for several hours before specimens were fractured. The fracture test was carried out *in situ* in the refrigerator, so that no temperature disturbances arose at this juncture. Before testing, the top surface of the ice block was smoothed using a sharp knife so that the specimen conformed to the geometry shown in Fig. 1, and the ice thickness was measured using calipers.

The time required to freeze the ice completely on a specimen was measured in some cases, this being achieved both by visual observation and by use of a thermocouple located at different heights above the substrate surface.

Testing variables were ice thickness, ice making temperature, testing temperature and the rate of pressurization. The latter was not a precisely controlled quantity but was categorized as "fast" (time to failure 0.02 to 0.03 sec), "standard" (0.07 to 0.10 sec), "slow" (0.4 to 0.6 sec) or "very slow" (0.7 to 0.9 sec).

3. Results

3.1. Description of ice specimens

The physical condition of the ice clearly exerts an influence over the fracture results and will therefore be considered here. The time required to freeze the ice varied according to the ice thickness, the making temperature and the nature of the substrate. Deliberate changes in the time to freeze were also introduced by insulating the sides of the specimen and mould ("insulated specimens") so that all heat abstraction from the liquid water occurred through the base block. Results for these tests are shown in Table I.

Ice made at $-5°$ C was transparent, with vertically elongated bubbles of air near the top of the casting. There was always a bubble-free zone (BFZ) adjacent to the substrate, and this is true of all specimens regardless of temperature. Centrally, at the top, there was usually a core of fine bubbles above which the upper surface was raised in a conical projection. Both these latter features were produced during the final stages of freezing.

TABLE I Times (min) to completely solidify the ice

Substrate	Temperature (° C)	Ice thickness (mm)		
		5	8	12
Titanium	−20	7	10	18
Stainless steel	−20	–	8	–
Titanium	−5	36	60	103
Stainless steel	−5	–	50	–
Insulated Ti	−5	90	115	148

The ice-formation sequence was as follows: (1) rapid freezing at the metal substrate surface; (2) simultaneous growth of ice crystals from the bottom and sides of the mould; (3) rejection of residual dissolved air as bubbles ahead of the growth front, the bubbles becoming entrapped; (4) ice formation on the upper surface proceeding from the edges inward; and (5) final solidification of the central pool of water at the surface. Water which had not been boiled produced similar ice, but with more elongated bubbles.

Ice made at $-20°$ C was normally cloudy with small bubbles, except for the BFZ of 1 to 2 mm at the substrate surface. Ice made from tap water, or dilute salt solutions, was opaque whether made at -5 or $-20°$ C. The crystal grain dimensions lay in the range 2 to 5 mm for ice made at $-5°$ C and 1 to 2 mm for ice made at $-20°$ C.

3.2. Observations of fracture mode

Distilled water ice, tested in the temperature range -5 to $-20°$ C, fractured cohesively regardless of substrate. The fracture initiated at the upper edges of the PTFE disc and formed an inverted cone which intersected the cylindrical surface of the ice block anywhere between 1 and 4 mm above the substrate. The cones were more shallow for stainless steel substrates than for titanium and anodised aluminium. For thin ice layers, the cones broke through the top surface of the ice block.

At temperatures between -5 and $0°$ C, a transition was observed from cohesive to adhesive failure. Pure adhesive failure did not occur with distilled water ice, but a significant proportion of the specimens exhibited some regions of interfacial separation in this temperature range. The tran-

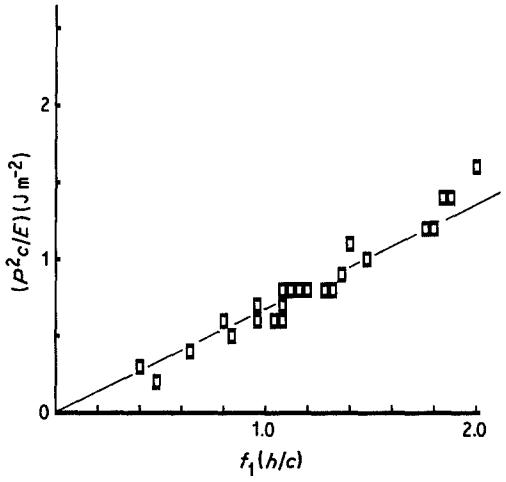

Figure 2 Plot to determine fracture energy $2\mathscr{T}$, which is equal to the slope of the line. Ice made and tested at $-5°$ C; stainless steel substrate. Standard pressurization rate.

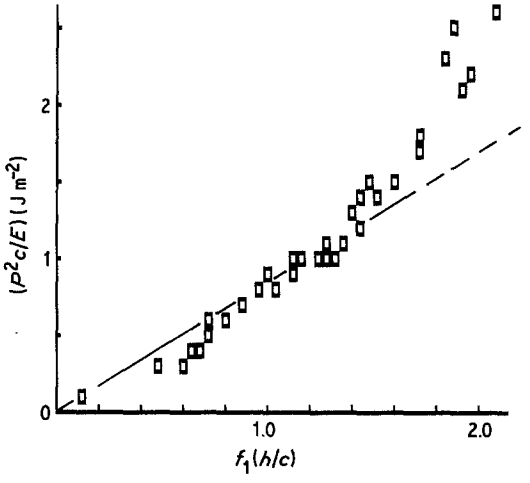

Figure 3 As Fig. 2 but for titanium substrate.

sition behaviour was found above $-3°$ C for ice on stainless steel and above $-2°$ C for titanium substrates. At very slow pressurization rates (fracture in 0.7 to 0.9 sec) the transitional behaviour began just above $-5°$ C for both Ti and steel substrates. Sodium fluoride solutions, at concentrations ranging from 0.1 to 1.0%, exhibited a much more definite transition, and fracture above $-5°$ C was always adhesive. Below this temperature a rapid transition to cohesive mode was observed over the temperature range -5 to $-7°$ C. These transitional effects are mirrored by the fracture-energy data reported below.

3.3. Fracture energies

The adhesive or cohesive fracture energy is given by the slope of a plot of $P_c^2 c/E$ against f_2 or f_1, respectively (see Equations 1 and 2). Such a plot is shown, for cohesive failure on stainless steel substrates, in Fig. 2. The theory is well borne out and the scatter is lower than is normal for brittle fracture tests. A well defined average slope, and the $2\mathscr{T}$ or G_c value, is thus obtained. There is a slight tendency in this plot for critical pressure to be low at small f_1 (small ice thickness) and high at large f_1, when compared with the average. This tendency becomes more evident in the data for Ti substrates shown in Fig. 3, and is a real effect which we shall discuss later. For the present, we will anticipate the conclusion that there is a small but genuine variation of slope, that is of $2\mathscr{T}$, with ice thickness. This variation is shown in Figs. 4 and 5 for titanium substrates and different pressurization rates. The effect is more pronounced at higher rates. In the data plots that follow, of $\mathscr{T}$ against temperature of testing, the $\mathscr{T}$ value used is that applying over the range $1.0 < f_1 < 1.5$.

The variation of $2\mathscr{T}$ or θ with temperature of testing is shown in Figs. 6 and 7. For these experiments the ice was always made at $-20°$ C to ensure consistency of results when tested at higher temperatures. Fig. 6 shows data for titanium substrates and two testing rates: standard and very slow. Below $-5°$ C the value of $2\mathscr{T}$ is independent of temperature, at 0.70 to 0.75 J m^{-2} for very slow pressurization and slightly higher (0.7 to 0.9 J m^{-2}) for standard rate. Above $-5°$ C the data becomes more scattered, and the mode of fracture tends towards adhesive with a corresponding decrease in fracture energy. The points for very

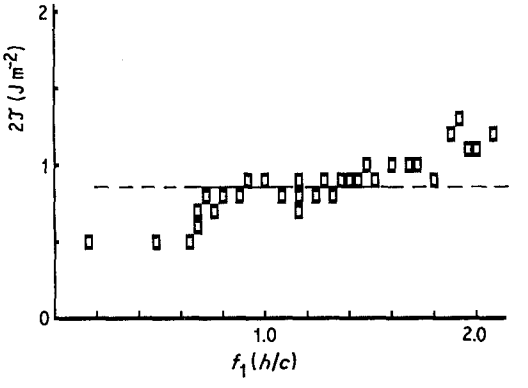

Figure 4 Variation of cohesive fracture energy with ice thickness. Titanium substrate. Ice made and tested at $-5°$ C. Standard pressurization rate.

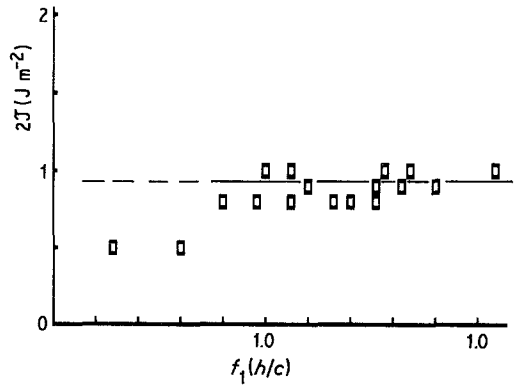

Figure 5 As Fig. 4 but at slow pressurization rate.

slow pressurization in this temperature range, fall below those for standard rate.

With stainless steel substrates (Fig. 7) the same behaviour is observed, the drop in fracture energy with rising temperature above $-5°$ C being better defined than for Ti substrates. Most significantly, the low-temperature value of $2\mathcal{T}$ is smaller for steel than for Ti, standing at 0.44 to 0.53 J m^{-2} for very slow pressurization, and 0.6 to 0.8 J m^{-2} for higher rates.

The effects of substrate, pressurization rate and other variables are summarized pictorially in Fig. 8 which shows the low-temperature (below $-5°$ C) data for $2\mathcal{T}$ plotted against a notional pressurization-rate scale. Included on this plot are points for anodised aluminium, and for Ti with the freezing rate deliberately slowed by insulation of the specimen. A clear pattern of behaviour emerges which can be summarized as follows:

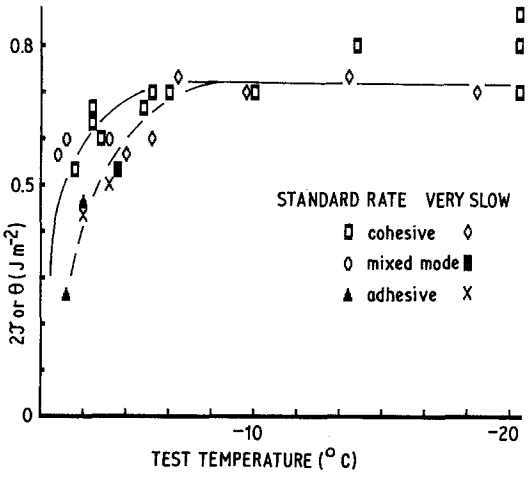

Figure 6 Variation of failure energy with test temperature for titanium substrates at two different pressurization rates as shown. Ice made at $-20°$ C.

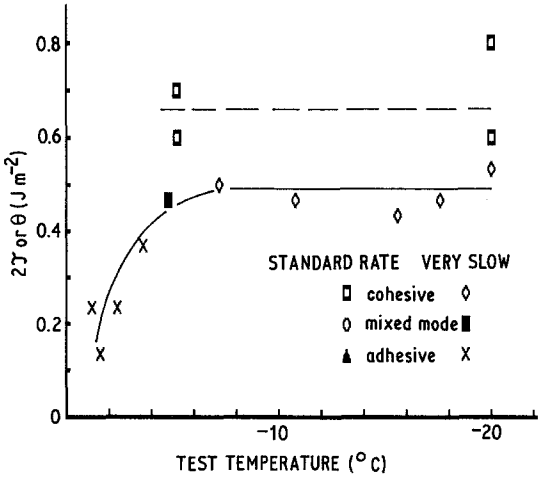

Figure 7 As Fig. 6 but for stainless steel substrates.

(1) The effect of rate of testing is more pronounced for those conditions under which $2\mathcal{T}$ is low;

(2) the values for $2\mathcal{T}$ converge as the rate increases;

(3) high $2\mathcal{T}$ values result from high ice-making temperatures and slow freezing rates. The consistently higher values for Ti substrates appear to stem from the slower cooling obtained with this material (see Table I).

To confirm the influence of cooling rate, data on Ti specimens are shown in Fig. 9. To obtain these results, account was taken of the difference in $\mathcal{T}$ arising from different ice thicknesses and illustrated in Figs. 4 and 5, together

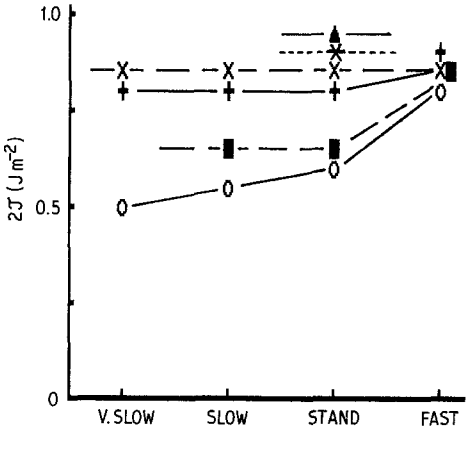

Figure 8 Effect of testing rate on cohesive fracture energy. From top to bottom: insulated Ti specimens; anodised Al; titanium at $-5°$ C, titanium at $-20°$ C; stainless steel at $-5°$ C; stainless steel at $-20°$ C. (Temperatures refer to both making and testing conditions.)

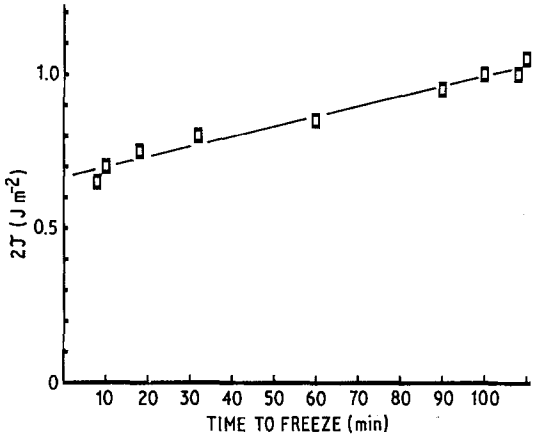

Figure 9 Effect of freezing time on $2\mathscr{T}$ for Ti substrates. All tests at $-5°$ C.

with the times to freeze different thicknesses of ice. A smooth curve demonstrates the direct influence of freezing rate on the measured $\mathscr{T}$ values. Similar results are obtained with stainless steel substrates, but these data do not fall on the same curve as for Ti. This indicates that cooling rate is not the only variable affecting fracture energy.

3.4. Fracture energies for salt solutions

The data from these tests are displayed in Figs. 10 and 11. When sodium fluoride is added to the water, the main effect is on the cohesive–adhesive transition. The transition temperature is reduced

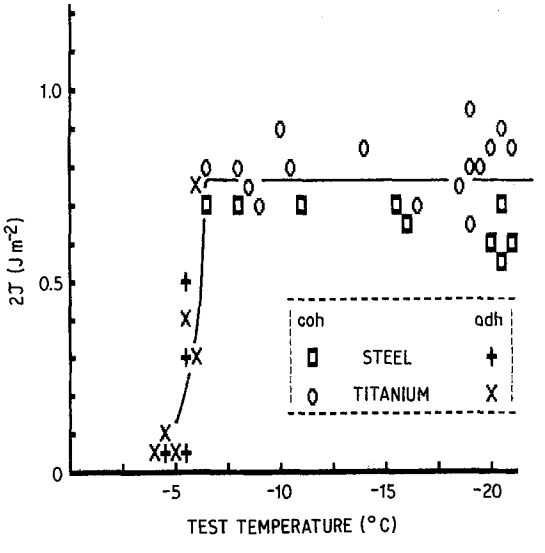

Figure 10 Dependence of failure energy on test temperature for 0.1% and 0.2% NaF solutions (not differentiated) on titanium and stainless steel substrates. Standard pressurization rate. Ice made at $-20°$ C.

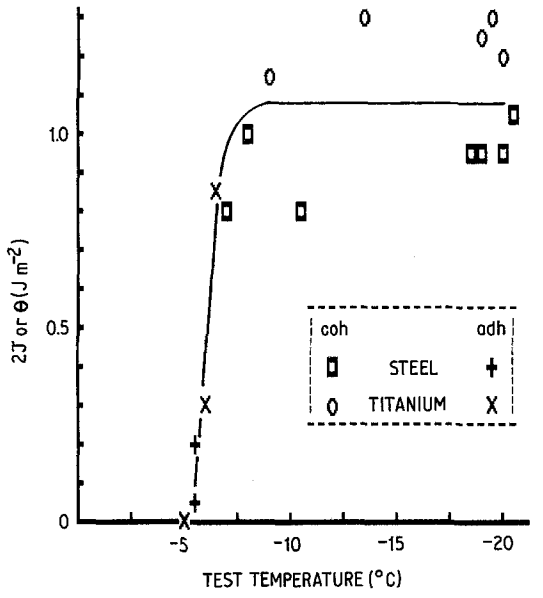

Figure 11 As Fig. 10 but for 1% NaF solution.

to $-6.5°$ C at 0.1 to 0.2% concentration, and to about $-8°$ C for 1.0% concentration. The transition is also greatly sharpened, with θ falling to zero at $-5°$ C. The other effects of note are the persistent differences between Ti and steel substrates, Ti again giving higher $\mathscr{T}$ values, and the significantly larger fracture energy obtained at the relatively high salt concentration of 1.0%.

Attempts to repeat these results using sodium chloride as the solute failed since no adhesion was obtained (zero θ) over the range of temperatures down to $-20°$ C even at low salt concentrations.

4. Discussion

4.1. The effects of ice-formation conditions on cohesive fracture energy

Most of these effects can, it transpires, be traced to the bubble content of the ice. Bubble formation in ice has been studied by Carte [15], who suggests that bubbles form ahead of the growth front when dissolved air concentrations reach a supersaturation of some 30-fold. Maeno [16] draws attention to the role of nucleating particles in their formation.

The effect of the bubble-free zone (BFZ) is demonstrated dramatically in Fig. 12 where the value of $2\mathscr{T}$ at $-5°$ C is plotted against the ratio of BFZ height to total specimen thickness for specimens with different substrates and rates of freezing. The residual scatter is due, in part at least, to rate of testing variations. It is clear that the major effects of substrate, cooling rate and

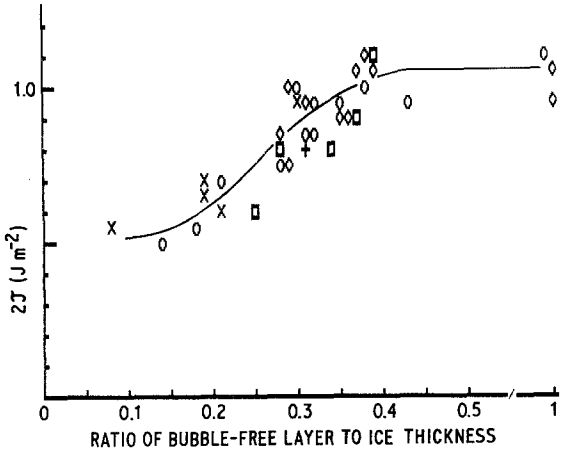

Figure 12 Effect on bubble-free zone on cohesive fracture energy. Various metallic substrates and freezing times. Ice made and tested at -5° C.

ice thickness arise through changes in the BFZ induced by these variables. We find in particular that: (1) slow freezing of the ice enables the air to diffuse away from the growth front and delays the onset of bubble formation. Thin ice specimens freeze more rapidly than thick ones, giving rise to a thickness dependence of the BFZ and of fracture energy; (2) substantially bubble-free ice made by slow cooling on stainless steel has the same high fracture energy as ice formed on a titanium substrate, as also does ice formed on stainless steel bonded to titanium instead of brass blocks; (3) a surface not "finished" by rubbing with silicon carbide paper, namely anodised aluminium, gives a large BFZ, and substrates deliberately contaminated with alumina or silicon carbide particles give small BFZ and low fracture energy; (4) ice made at -20° C always has a thin BFZ and exhibits lower fracture energies than ice formed at -5° C (tests being carried out at the same temperature); (5) ice frozen on to polymeric substrates has been tested in a series of experiments not reported here. These specimens usually have a large BFZ on account of the low thermal conductivity of the substrate. When fracture is cohesive, the $\mathscr{T}$ values correspond to the highest values obtained in this study.

Returning to Fig. 12, we see that clear ice exhibits a cohesive fracture energy, $2\mathscr{T}$, at -5° C of $1.0 \pm 0.1\,\mathrm{J\,m^{-1}}$, and this must be taken as the true value. Earlier data show no variation of this figure over the temperature range -5° to 20° C. The effect of bubbles on $2\mathscr{T}$ might at first be attributed to a direct alteration of fracture energy, e.g. a weakening of the ice. This cannot be the case in our experiments, however, since $2\mathscr{T}$ is measured at initiation which always occurs in the BFZ, i.e. in clear ice. The lower values found for $2\mathscr{T}$ when the BFZ forms less than 40% of the total specimen thickness are plainly due to the bubble ice being more compliant than clear ice. In the calibration of $\mathscr{T}$, the ice is considered to be homogeneous with a Young's modulus of 8.5 GN $\mathrm{m^{-2}}$, and if any region of the ice has a smaller effective modulus, this will result in an underestimation of fracture energy. Since $\mathscr{T}$ is linearly related to E in Equation 1, it follows from Fig. 12 that the bubble-ice has an effective modulus only half that for 100% bubble-free ice.

The density of bubble-ice was measured by weighing in air and in *n*-heptane at -5° C. Densities in the range 0.892 to $0.907\,\mathrm{g\,cm^{-3}}$ were found, compared with a density of $0.917\,\mathrm{g\,cm^{-3}}$ for bubble-free ice. It is obvious, therefore, that by the rule of mixtures the Young's modulus of bubble-ice cannot be more than a few per cent lower than that of clear ice. Yet the apparent reduction of modulus is some 50%.

The probable answer to this dilemma is that the bubble-ice lacks mechanical coherence under load, perhaps undergoing micro-cracking as the specimen is pressurized before failure. Bubbles, and possibly intergranular micro-bubbles, could provide nuclei for such micro-cracking. The overall effect, of course, would then be the same as that of enhanced mechanical creep, and the apparent modulus akin to a creep modulus. This idea is supported by the observation noted in Fig. 8, that fracture energy (and thus effective modulus), tends to a consistently high value as the rate of testing increases. At high speeds of testing, micro-cracks would have insufficient time to form or grow, and the effective modulus of the bubble-ice would be similar to that of clear ice. Although micro-cracking is here represented as a cause of enhanced creep, it must be clearly differentiated from true creep arising from grain-boundary sliding or crystallographic mechanisms. Such true creep may reduce the apparent $\mathscr{T}$ value by reducing the effective modulus but may also have the opposite effect of increasing $\mathscr{T}$ by energy dissipation. The effects of micro-cracking, lowering $\mathscr{T}$ and of true creep, enhancing $\mathscr{T}$, may of course manifest themselves over different time-scales and this question is under investigation.

4.2. The magnitude of the cohesive fracture energy

While the failure energy for adhesive breakdown varies from zero upwards according to conditions, the cohesive fracture energy is fairly constant at 0.9 to 1.1 $J\,m^{-2}$. For specimens containing air bubbles this figure is artifically depressed, whilst for salt solutions $2\mathscr{T}$ appears to rise (a value of 1.13 $J\,m^{-2}$ having been observed in this work). How do these figures compare with data produced by other workers?

Goodman [11] summarizes values obtained for G_c (the linear theory equivalent of $2\mathscr{T}$) by various authors and shows them all lying in the range 0.6 to 2.3 $J\,m^{-2}$ with the variability in any one study lying between 15 and 50%. Our data lie well within this range, perhaps tending towards the lower end of the range on account of the strictly plane-strain conditions of our test which inhibit plastic flow. The situation is not as simple as Goodman's summary suggests, however. At slow testing rates the G_c value appears to rise to very high values and becomes much more temperature dependent than at high testing rates. Miller [24] plots K_{IC} against temperature for loading rates varying between 0.5 and 480 mm sec^{-1} and shows a linear rise with falling temperature which is small for fast tests but which shows a two-fold increase between 0° C and − 50° C for the slowest experiments. The corresponding G_c or $2\mathscr{T}$ values for low temperatures and slow rates rise as high as 17 $J\,m^{-2}$, due to plastic flow in the ice. Goodman and Tabor [10] show similar data for G_c showing values as high as 38 $J\,m^{-2}$ for the lowest rates and temperatures.

Our own tests are all carried out at relatively high testing rates and yield data at the low end of the ranges observed by others. More recent experiments, which will be published separately, indicate that as the rate of testing is lowered, we too observe an increase in $2\mathscr{T}$. However, we have never observed values in excess of 3 $J\,m^{-2}$ and believe that our results represent the plane-strain limit of fracture energy in ice. This is a reasonable supposition because of the highly constrained configuration of a totally enclosed crack, which minimizes plastic deformations around the crack tip.

4.3. The cohesive–adhesive transition

The basic nature of a cohesive–adhesive transition can be understood in terms of the generalized theory of fracture developed by Andrews and co-workers [2, 17, 18]. The theory gives the fracture energy of a solid as,

$$2\mathscr{T} = 2\mathscr{T}_0\,\Phi(\dot{c}, T, \epsilon), \tag{5}$$

and the corresponding adhesive failure energy as,

$$\theta = \theta_0\,\Phi(\dot{c}, T, \epsilon), \tag{6}$$

the latter equation applying when the adhesive material is the solid in question and the substrate is ideally elastic (a condition which is effectively satisfied if the substrate is much more rigid than the "adhesive"). The parameters $2\mathscr{T}_0$ and θ_0 are the energies actually required to separate unit area of inter-atomic bonds across the fracture plane in cohesive and adhesive fracture, respectively. In the simplest case, these quantities are (twice) the surface energy of the solid and the interfacial energy of the adhesive bond, respectively. The "loss function", Φ, is a function of the rate of crack propagation, $\dot{c}$, of temperature T, and of the overall level of strain in the system, ϵ. Each of these variables exerts its effect by altering the "hysteresis ratio" of the solid, that is, the fraction of energy lost in a strain cycle. For perfectly elastic materials, Φ is unity and the fracture energy equals the surface energy (as proposed by Griffith [19]). For most real solids, however, $\Phi > 1$ and $\mathscr{T} > \mathscr{T}_0$, or $\theta > \theta_0$. Provided the substrate is rigid, the Φ function is the same for cohesive and adhesive failure, and this has been demonstrated experimentally [1, 2].

A transition from cohesive to adhesive failure can now be represented very simply as a point where, as a consequence of some variable of test, the interfacial energy, θ_0, decreases below the surface energy term, $2\mathscr{T}_0$. Since surface energy is relatively insensitive to temperature, this normally means that the interfacial energy is changing with the test variable in question. Such transitions have been studied for epoxy resins bonded to metals and glass [3, 20] where an originally cohesive mode can be changed to adhesive failure by exposing the bond to water for a long enough period of time. This causes hydrolysis of the interfacial atomic bonds and a progressive decrease in θ_0. Nothing happens, however, until the situation is reached where $2\mathscr{T}_0$ and θ_0 are equal. At this juncture, a sudden switch to the adhesive mode ensues.

Applying the same reasoning to the present case, we propose that the transition observed with

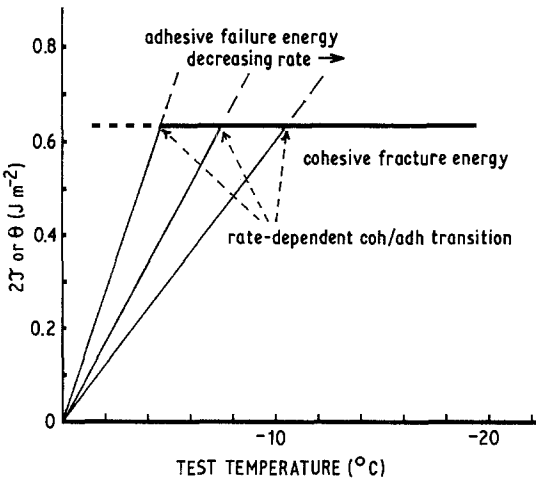

Figure 13 Schematic diagram illustrating the cohesive–adhesive failure transition and its possible origin.

ice arises because the interfacial bonding decreases in strength as temperature rises and becomes comparable to the surface energy of ice at the temperature of transition (see schematic diagram in Fig. 13). If this is true, we must explain two things. Firstly, why is the interfacial energy greater than the surface energy at temperatures below the transition, and secondly, what causes the interfacial energy to decrease with rising temperature?

The atomic bonding at the interface is essentially the same as that within the ice, namely hydrogen bonding. This is because all the metals have stable oxide layers which, in turn, are hydrated with bound and adsorbed water. The interfacial bonding will, however, be spatially less regular than within the ice crystal lattice, and the "melting point" of the interfacial layer will be lower than that of the ice lattice.

At sufficiently low temperatures, therefore, we would expect the mechanical strength of the interface to be similar to that of the solid ice, and this may be a sufficient condition to ensure cohesive failure. Strictly, according to the simple theory outlined above, θ_0 must *exceed* $2\mathscr{T}_0$ for the cohesive mode to be observed. But complicating this simple picture is the existence of interfacial stresses due to differential thermal contraction, and these stresses (being relieved by any vertical component of crack propagation) will help to drive a cohesive crack rather than an interfacial one. Mantovani and Valeri [21] have considered the role of such stresses in cracking and considered them negligible above -25° C. We estimate an average unrelaxed shear stress of between 1.5 and 2.2 kN m^{-2} at -5° C, and between 6.2 and 8.9 kN m^{-2} at -20° C, according to substrate. These stresses are low compared with the tensile strength of ice [22], but may be sufficient to favour cohesive failure when $\theta_0 \sim 2\mathscr{T}_0$. Quite apart from the magnitude of such stresses, the distribution of stress around an interfacial crack will be asymmetrical due to the change of elastic constants across the interface, and this again is likely to favour cohesive fracture as long as the interfacial energy is not significantly less than the solid surface energy.

As the temperature rises towards 0° C, however, the disordered layer at the interface (which can be viewed as a crystal containing a high concentration of defects), must undergo melting, thus producing a rapid fall in θ_0 and the observed transition to an adhesive failure mode. This picture accords with the idea of a "liquid-like" layer at the interface, proposed by Jellinek [13] and discussed by Landy and Freiberger [23]. This layer is normally considered to be present at temperatures down to -10° C or even lower, and Jellinek's data show a cohesive–adhesive transition in shear tests at -13° C. This discrepancy is almost certainly due to the effect of rate on the shear strength of the disordered layer. Jellinek shows this strength increasing linearly with shear-rate and Fig. 6 of the present paper suggests that the failure energy rises more slowly as temperature falls when the rate of testing is low. The transition temperature thus falls as the rate of testing decreases as shown in Fig. 13.

4.3. The influence of solutes

The cohesive to adhesive transition in NaF solutions may also be understood in terms of interfacial melting. The freezing points of the solutions used (-0.09, -0.18 and -0.83° C for 0.1%, 0.2% and 1.0% solutions, respectively) are not sufficiently different from that of pure ice to cause the lower and sharper transition observed in these specimens. On the other hand, there exists an ice/NaF eutectic which melts at -5.6° C. If the interfacial layer contains a high proportion of the eutectic phase, as is likely, the abrupt transition from cohesive to adhesive failure for the more dilute solutions, occurring at just this temperature, is well explained by interfacial melting. For the 1.0% solution the transition appears to start at the lower temperature of about -8° C, although the most rapid fall still occurs in the

range -5 to -6° C. The reduction in failure energy around -8° C is associated with a significantly higher value of $2\mathscr{T}$ than is found for pure ice or the more dilute solutions (1.2 to 1.3 J m^{-2} on Ti substrates, compared with 1.0 J m^{-2} for clear ice).

It is possible that this enhanced cohesive strength is also associated with eutectic formation, but in the grain boundaries of the bulk ice rather than at the interface. If normal bulk failure of ice involves any significant intergranular component, the presence of eutectic phase could obviously exert an influence.

We cannot advance a precise reason why the transition to adhesive failure begins some 2 to 3° C below the eutectic melting point, but the gradual fall in fracture energy between -8 and -6° C is not unlike that found in pure ice in the range -2 to -3° C. It can be argued, therefore, that when the eutectic is present in sufficient quantity, its disordered interface with the substrate behaves in a similar way to that of pure ice as the temperature rises to within 2 or 3° C of the relevant melting point. The collapse of fracture energy to zero at -5° C in the solutions then corresponds to the total melting of pure ice at 0° C. Because, however, the eutectic is present mainly as an enriched interfacial layer, the solutions can be mechanically tested at -5° C, while pure ice cannot be so tested at 0° C because of wholesale melting of the specimen.

Finally, the suggested role of the eutectic is borne out by the behaviour of NaCl solutions. In these materials we were unable to measure non-zero values of θ in the temperature range 0 to -20° C, and this would be expected since the ice/NaCl eutectic melts at -21° C.

5. Conclusion

The Andrews–Stevenson test has proved effective for the study of plane-strain cohesive and adhesive fracture in ice bonded to metallic substrates. The fracture energies are sufficiently well defined by this technique to enable us to observe significant differences in apparent fracture energy between different substrates and preparation conditions. Almost all of these differences can be attributed to the presence of a layer of bubble ice which is prone to time-dependent micro-cracking, thus altering the mechanical response of the ice specimen.

The test method is particularly useful in the study of the transition from cohesive to adhesive failure as the temperature is raised towards 0° C. This transition can be attributed to interfacial melting of a disordered, molecular-scale, layer immediately adjacent to the interface. In the case of salt solutions this layer is replaced by one containing a high concentration of a eutectic phase, whose melting dominates the transition behaviour.

Acknowledgement

The authors express their thanks to the Ministry of Defence (Royal Aircraft Establishment) for their financial support and encouragement of this research.

References

1. E. H. ANDREWS and A. J. KINLOCH, *Proc. Roy. Soc. (Lond.) A* **332** (1973) 385.
2. E. H. ANDREWS and A. STEVENSON, *J. Adhesion* **11** (1980)17.
3. E. H. ANDREWS, HE PINGSHENG and C. VLACHOS, *Proc. Roy. Soc. (Lond.) A* **381** (1982) 345.
4. E. H. ANDREWS and A. STEVENSON, *J. Mater. Sci.* **13** (1978) 1680.
5. P. V. HOBBS, "Ice Physics" (Clarendon Press, Oxford, 1974).
6. H. H. G. JELLINEK, *Proc. Phys. Soc. (Lond.)* **71** (1958) 797.
7. I. HAWKES and M. MELLOR, *J. Glaciology* **11** (1972) 103.
8. H. C. WU, K. J. CHANG and J. SCHWARZ, *Eng. Fract. Mech.* 8 (1976) 365.
9. L. W. GOLD, *Canad. J. Phys.* **41** (1963) 1712.
10. D. J. GOODMAN and D. TABOR, *J. Glaciology* **21** (1978) 651.
11. D. J. GOODMAN, "Physics and Mechanics of Ice", edited by P. Tryde (Springer Verlag, Berlin, 1980) p. 129.
12. H. W. LIU and K. J. MILLER, *J. Glaciology* **22** (1979) 135.
13. H. H. G. JELLINEK, *J. Colloid Interface Sci.* **25** (1967) 192.
14. L. W. GOLD, *Canad. J. Phys.* **36** (1958) 1256.
15. A. E. CARTE, *Proc. Phys. Soc. (Lond.)* **77** (1961) 757.
16. N. MAENO, in "Physics of Snow and Ice", edited by H. Oura, Proceedings of the International Confererence, Sapporo, Japan, 1966, Vol. 1, Part 1 (Hokkaido University, Sapporo, 1967) p. 207.
17. E. H. ANDREWS, *J. Mater. Sci.* 9 (1974) 887.
18. E. H. ANDREWS and Y. FUKAHORI, *ibid.* **13** (1978) 777.
19. A. A. GRIFFITH, *Phil. Trans. Roy. Soc. A* **221** (1921) 163.
20. E. H. ANDREWS and N. E. KING, *J. Mater. Sci.* **11** (1976) 2004.
21. J. MANTOVANI and S. VALERI, *Phil. Mag. A* **37** (1978) 17.

22. C. GANDHI and M. F. ASBHY, *Acta. Metall.* **27** (1979) 1565.
23. M. LANDY and A. FREIBERGER, *J. Colloid Interface Sci.* **25** (1967) 231.
24. K. J. MILLER, in "Physics and Mechanics of Ice", edited by P. Tryde (Springer Verlag, Berlin, 1980) p. 265.

Received 22 July
and accepted 14 October 1982